
Figures and figure supplements

Effects of common mutations in the SARS-CoV-2 Spike RBD and its ligand, the human ACE2 receptor on binding affinity and kinetics

Michael I Barton *et al*

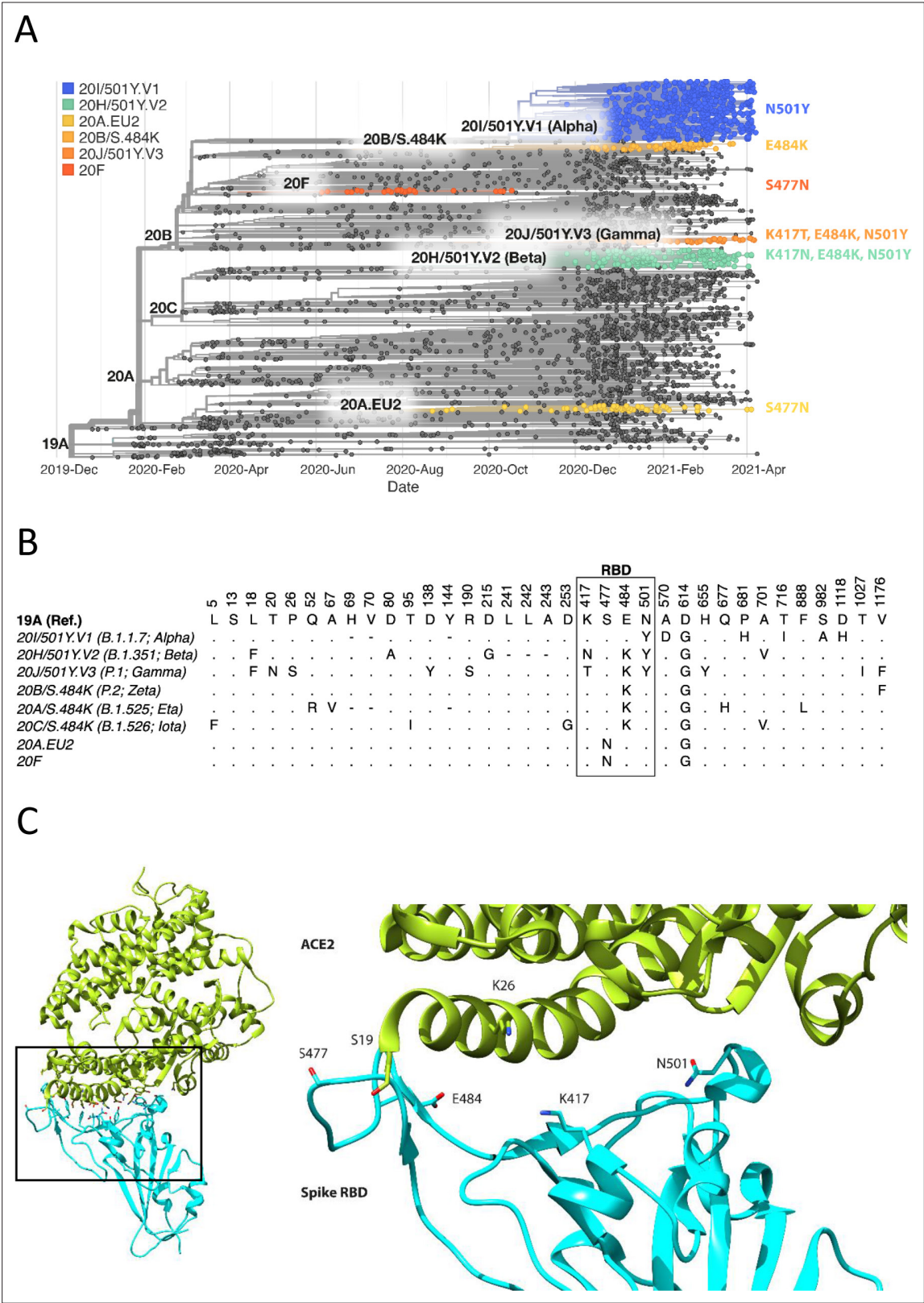


Figure 1. Spike RBD and ACE2 variants analysed in this study. **(A)** Phylogenetic tree illustrating the clades containing the RBD mutations investigated in this study. Constructed using TreeTime (Sagulenko et al., 2018) from the Nextstrain Global (Hadfield et al., 2018) sample of SARS-CoV-2 sequences from the GISAID database (Shu and McCauley, 2017) (accessed 15 April 2021, N = 4017). **(B)** Alignment illustrating the Spike residues that differ between SARS-CoV-2 variants, with the RBD mutants boxed. The variants are labelled with their clade designation from Nextstrain (Hadfield et al., 2021). **(C)** 3D ribbon diagram of the ACE2 protein (green) and the Spike RBD (cyan). Key residues are labeled: K26, S19, S477, E484, K417, and N501. The Spike RBD is shown in a stick representation, and the ACE2 protein is shown in a ribbon representation.

Figure 1 continued on next page

Figure 1 continued

2018) and/or PANGO lineage (**Rambaut et al., 2020**), where relevant. The RBD mutations were collated from CoVariants (**Hodcroft, 2021**) and Nextstrain. **(C)** The structure of human ACE2 (green) in complex with SARS-CoV-2 Spike RBD (cyan). The area enclosed by the box is shown enlarged on the right, with the residues mutated in this study labelled. Drawn using UCSF Chimera (**Pettersen et al., 2004**) using coordinates from PDB 6m0j (**Lan et al., 2020**).

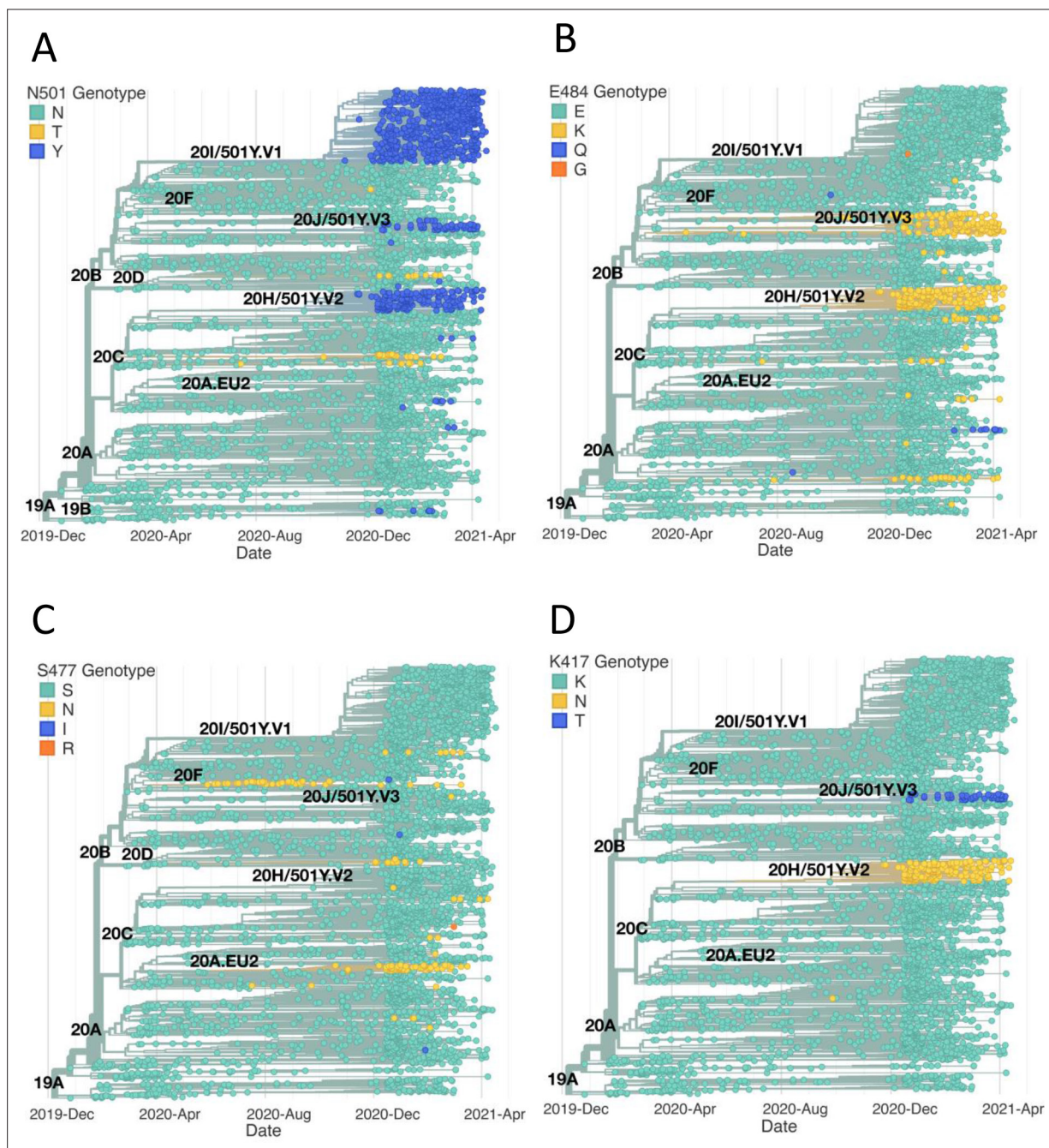


Figure 1—figure supplement 1. Emergence of the same RBD mutations in multiple SARS-CoV-2 clades. The figure highlights the SARS-CoV-2 clades containing RBD mutations investigated in this study. The phylogenetic trees were constructed as in **Figure 1A** from SARS-CoV-2 sequences accessed on 22 April 2021 (N = 3914). **(A)** N501Y has emerged independently in the three clades 501Y.V1, 501Y.V2, and 501Y.V3. Mutation to T at this position has also occurred frequently. **(B)** E484K has also been observed independently of its main progenitor clades 501Y.V2 and 501Y.V3. E484Q and E484G have also been observed. **(C)** S477N has been observed beyond clades 20 F and 20A.EU2. Mutations to I and R have also been occasionally observed at this position. **(D)** Mutations of K417 to N and T have been observed almost exclusively in the 20 H.501Y.V2 and 20 J.501Y.V3 clades.

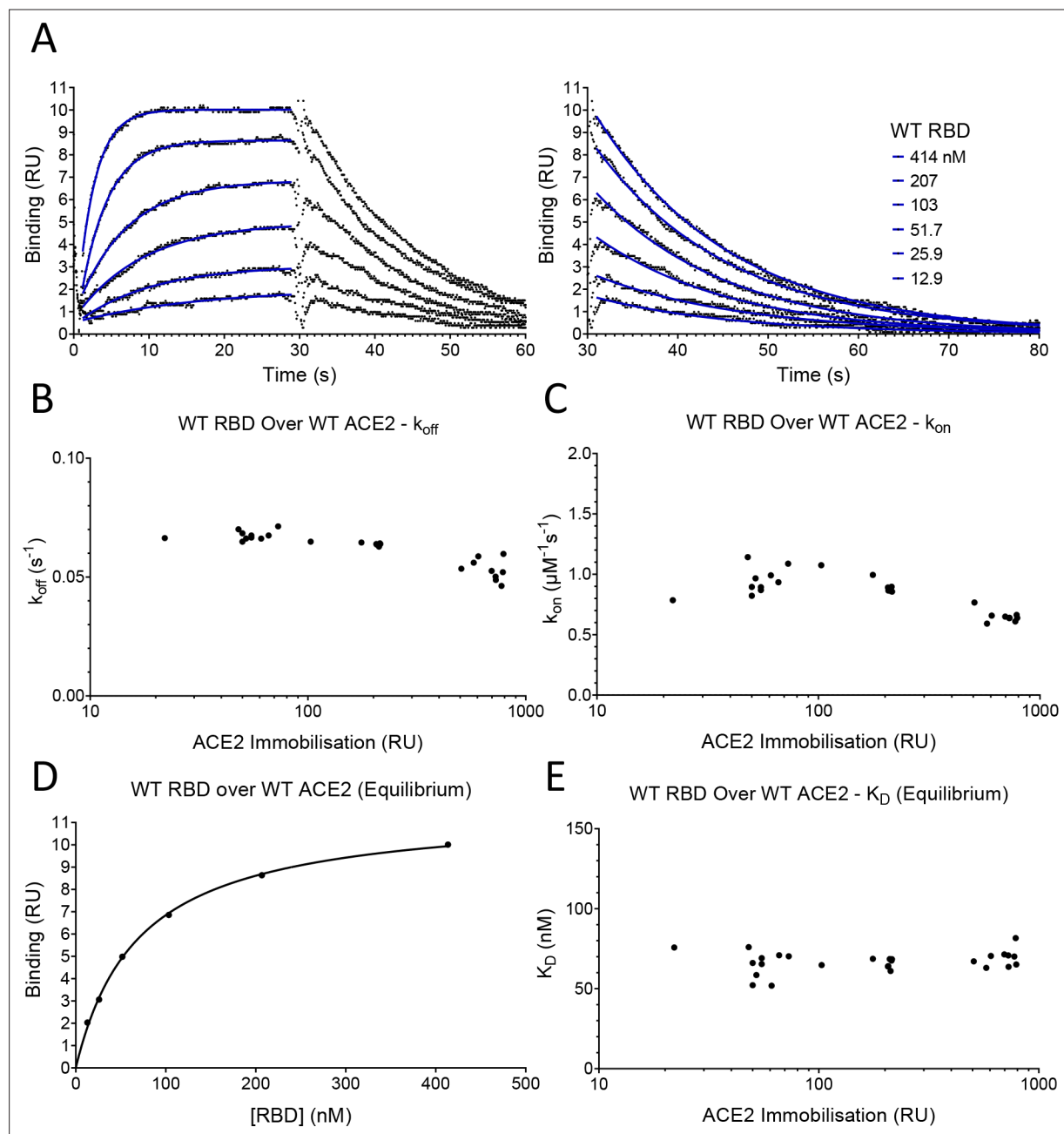


Figure 2. SPR analysis. **(A)** Overlay of traces showing association and dissociation when WT RBD is injected for 30 s at the indicated concentration over immobilised WT ACE2. The right panel shows an expanded view of the dissociation phase. The blue lines show the fits used for determining the k_{on} and k_{off} . The k_{on} was determined as described in **Figure 2—figure supplement 2**. The k_{off} **(B)** and k_{on} **(C)** values measured at different levels of immobilised ACE2 are shown. **(D)** The equilibrium K_D was determined by plotting the binding at equilibrium against [RBD] injected. Data from experiment shown in **(A)**. **(E)** The equilibrium K_D measured at different levels of immobilised ACE2 are shown.

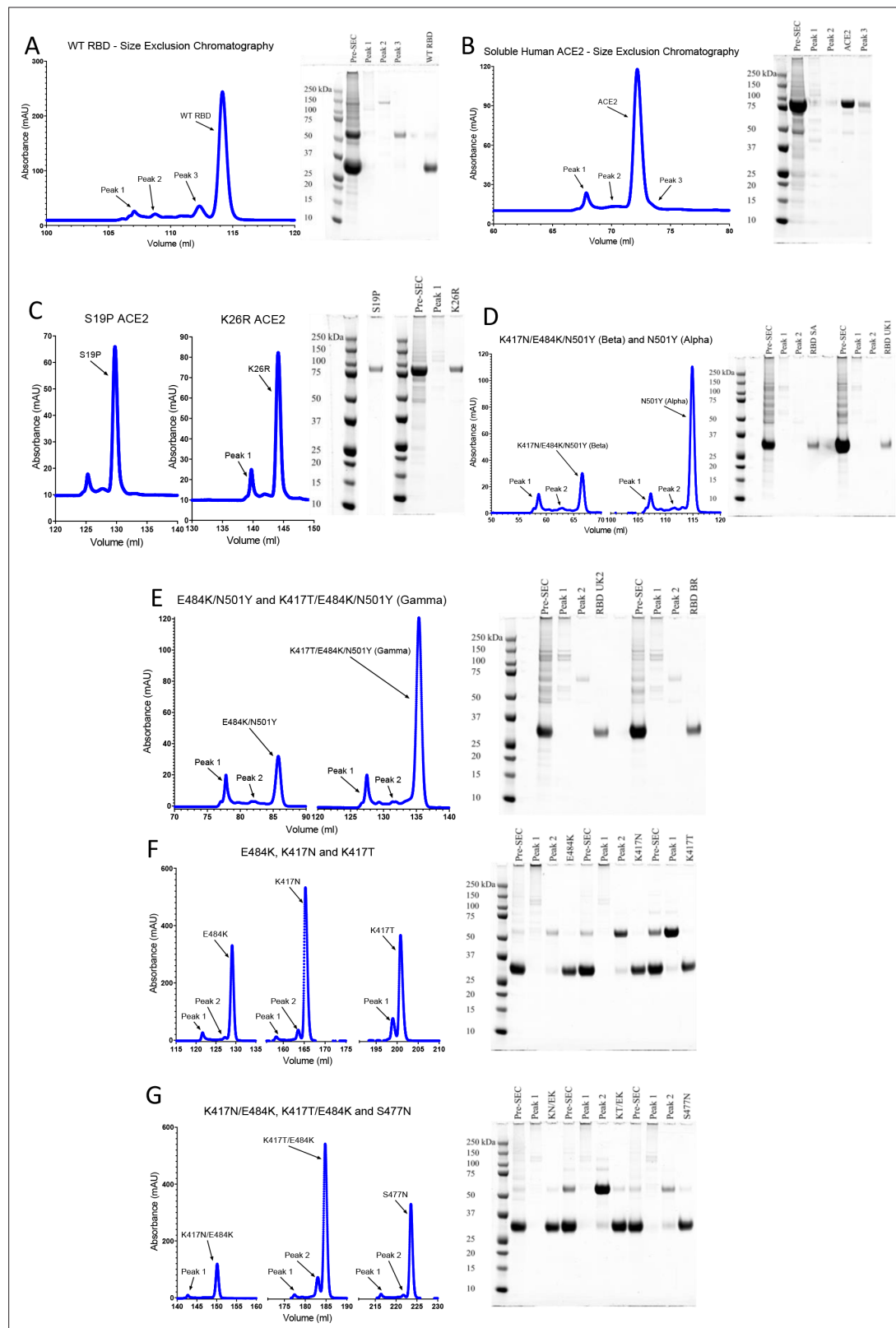


Figure 2—figure supplement 1. Protein purification. Size-exclusion chromatography traces of the indicated ACE2 and RBD proteins and reducing SDS-PAGE of the indicated peak fractions. UK2 refers to the VOC-202102-02 variants. In preparations of RBD, unidentified ~60 kDa contaminants were present at various levels, but always <5 % by densitometry.

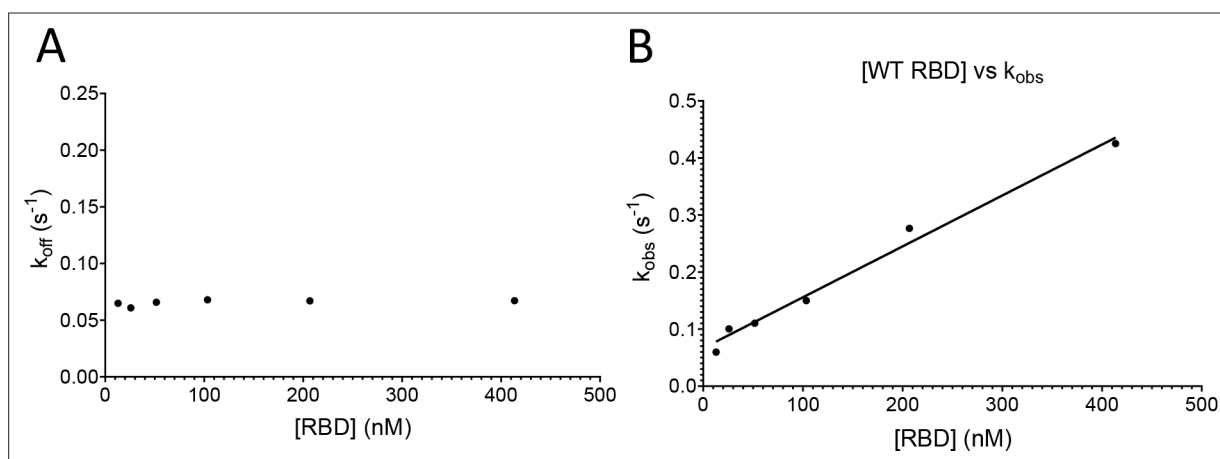


Figure 2—figure supplement 2. Determining the k_{on} and k_{off} . Analysis of data from the fits in **Figure 2A**. **(A)** A plot of k_{off} obtained for each injection versus [RBD]. **(B)** A plot of k_{obs} for each injection versus [RBD]. The line shows a constrained fit of the equation $k_{\text{obs}} = k_{\text{on}} \cdot [\text{RBD}] + k_{\text{off}}$, using the k_{off} obtained in **(A)**. The k_{on} was obtained from the slope.

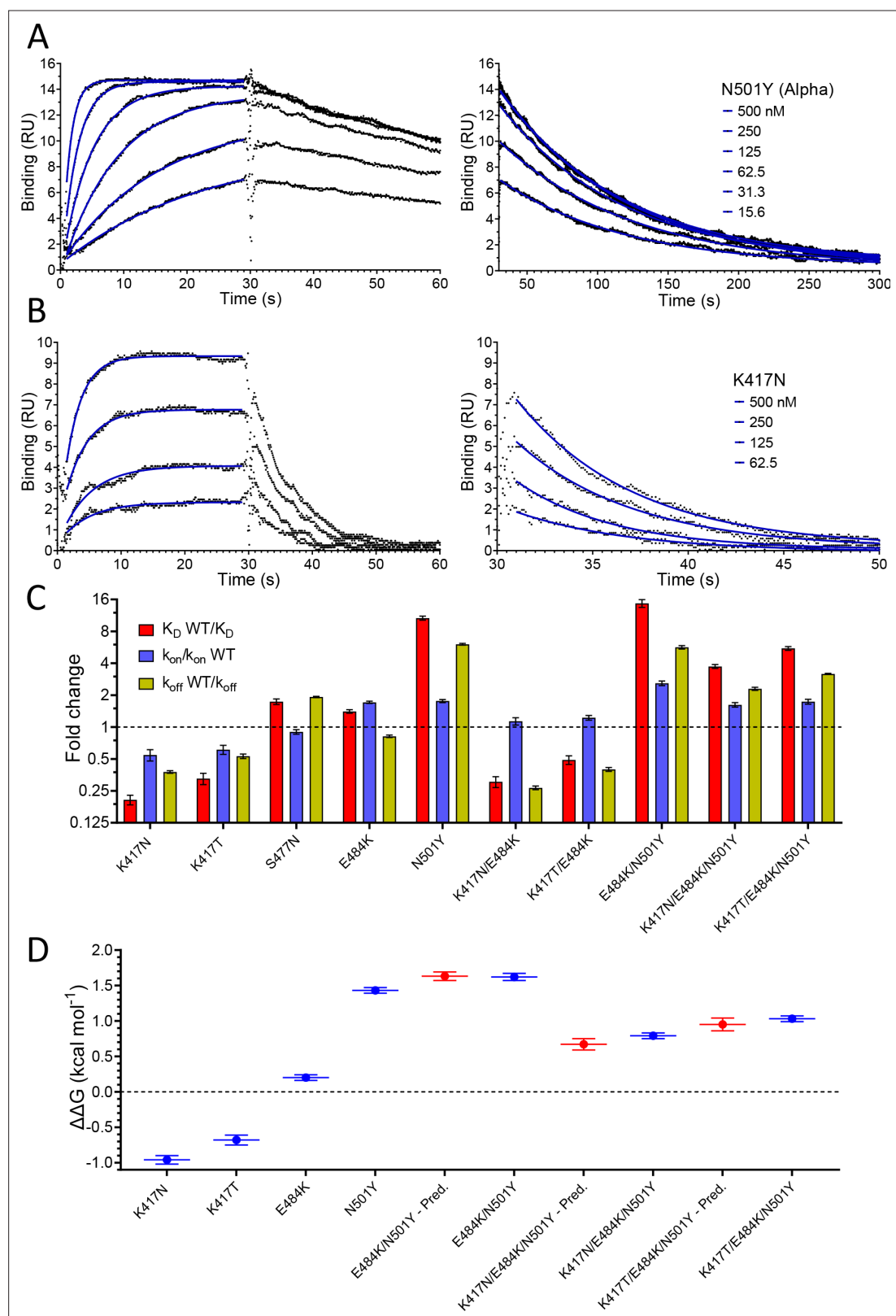


Figure 3. Effect of RBD mutations on binding to WT ACE2. Overlay of traces showing association and dissociation of N501Y (**A**) and K417N (**B**) RBD variants when injected at a range of concentrations over immobilised WT ACE2. The right panels show an expanded view of the dissociation phase. The blue lines show fits used for determining the k_{on} and k_{off} . (**C**) The fold change relative to WT RBD of the calculated K_D , k_{on} , and k_{off} for binding of the indicated RBD variants to immobilised WT ACE2 (error bars show SD, $n = 3$). Representative sensorgrams from all mutants shown in **Figure 3—figure**

Figure 3 continued on next page

Figure 3 continued

supplement 2, and the mean values from multiple repeats are in Table 1. **(D)** The blue lines show the measured $\Delta\Delta G$ for indicated RBD variants. The red lines show the predicted $\Delta\Delta G$ for the RBD variants with multiple mutations, which were calculated by adding $\Delta\Delta G$ values for single mutation variants (error bars show SD, $n = 3$).

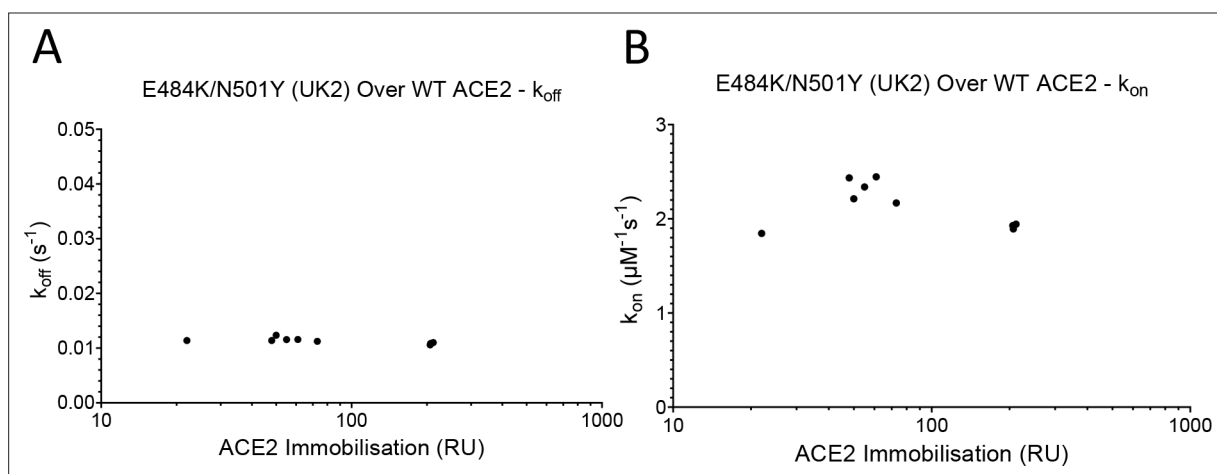


Figure 3—figure supplement 1. Mass transport controls for RBD. The k_{off} (A) and k_{on} (B) for E484K/N501Y (UK2) RBD binding WT ACE2 at a range of surface immobilisations ($n = 12$). UK2 refers to VOC-202102–02.

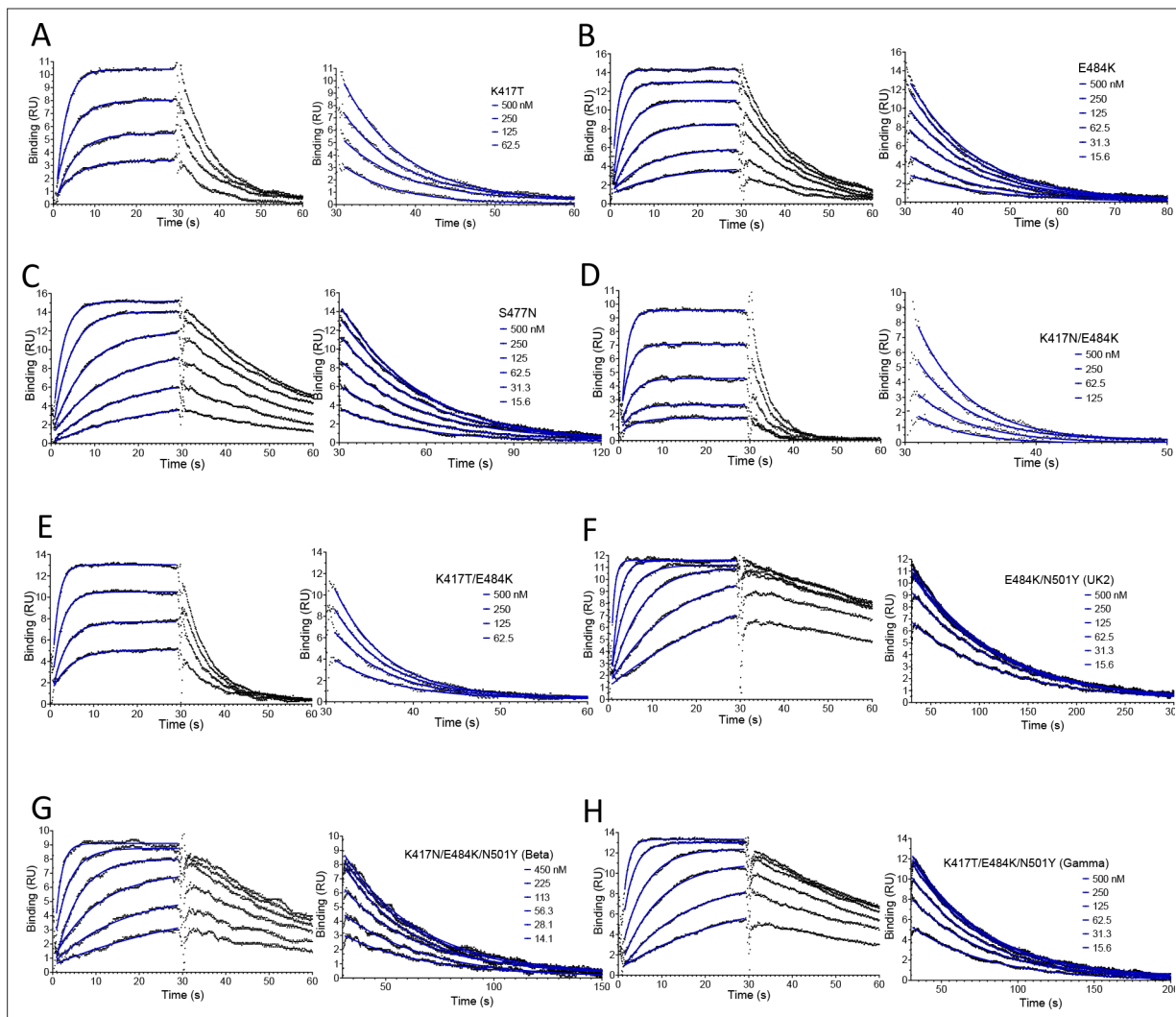


Figure 3—figure supplement 2. Representative SPR data for RBD variants binding to WT ACE2. Binding traces for the indicated RBD variants injected at different concentrations over immobilised WT ACE2. The right panels show an expanded view of the dissociation phase. The blue lines show fits used for determining the k_{on} and k_{off} . UK2 refers to the VOC-202102-02 variant.

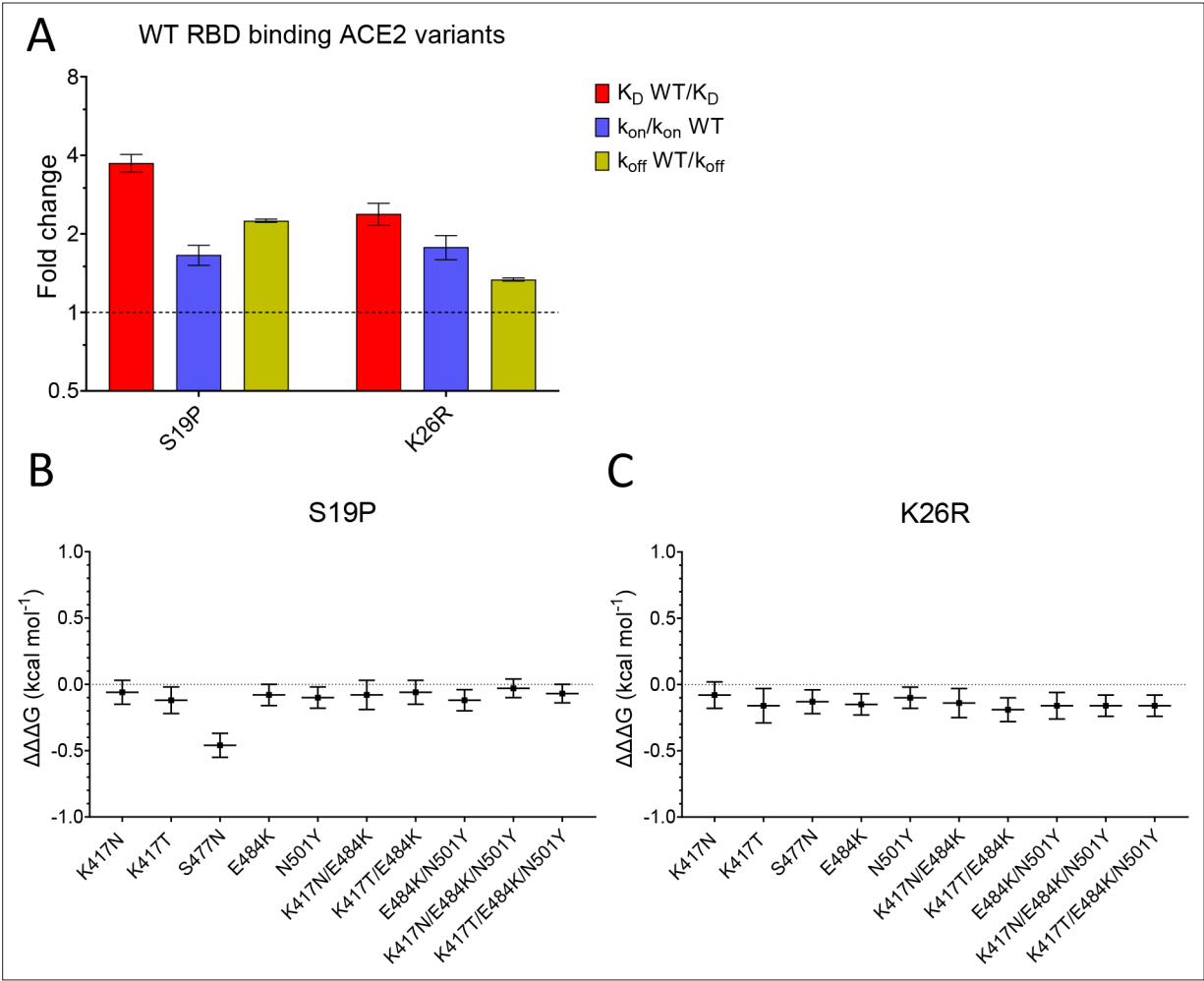


Figure 4. Effect of mutations in ACE2. **(A)** The fold change relative to WT ACE2 of the calculated K_D , k_{on} , and k_{off} for the interaction of WT RBD and the indicated ACE2 variants (error bars show SD, $n = 3$). **(B, C)** Show the difference ($\Delta\Delta G$) between the measured and predicted $\Delta\Delta G$ for S19P **(B)** and K26R **(C)** ACE2 variants binding to the indicated RBD variants, calculated from data in Table 2. The predicted $\Delta\Delta G$ values for each variant RBD/variant ACE2 interaction were calculated from the sum of the $\Delta\Delta G$ for the ACE2 variant binding WT RBD and the $\Delta\Delta G$ for the RBD variant binding WT ACE2 (Table 2).

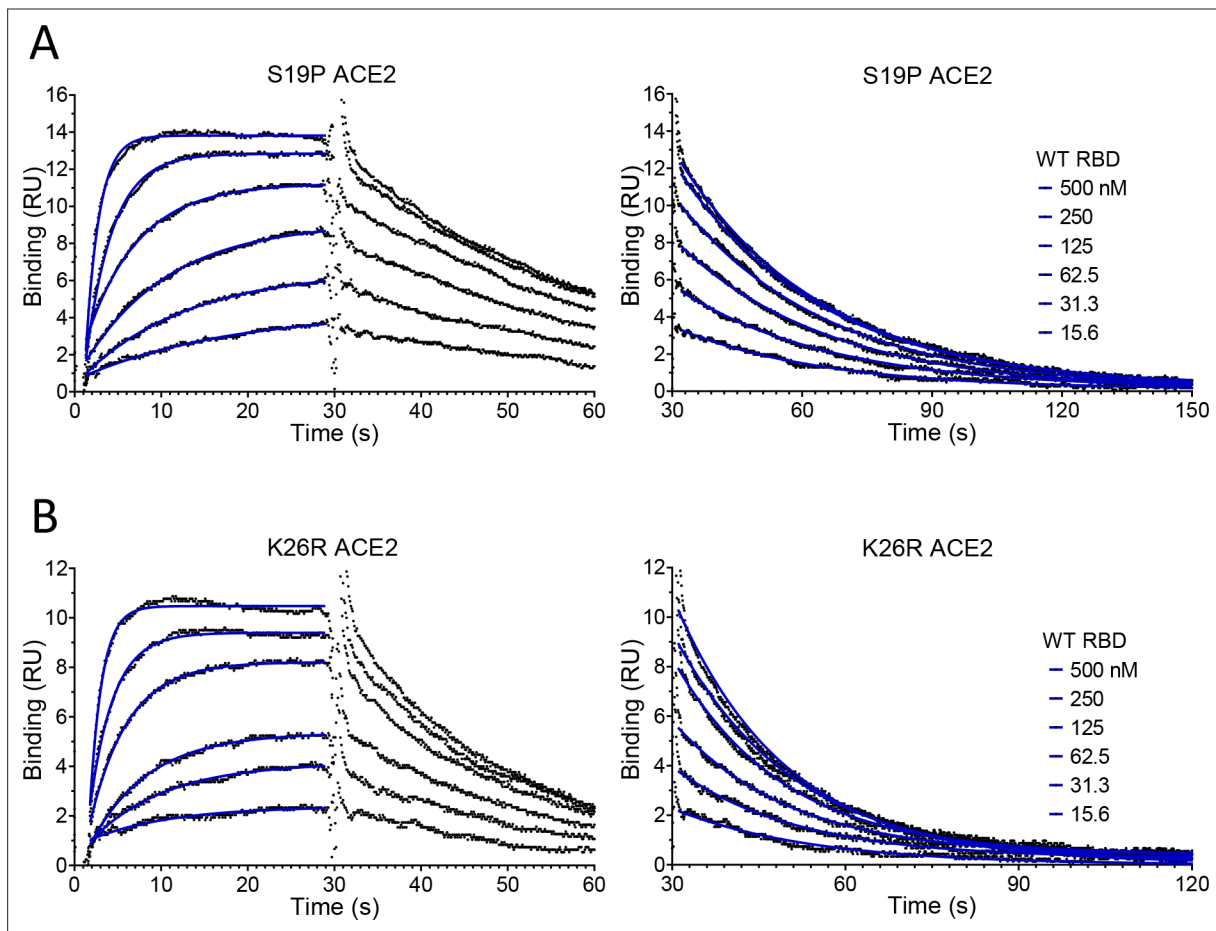


Figure 4—figure supplement 1. Representative SPR data for WT RBD binding ACE2 variants. Binding traces for the WT RBD injected at different concentrations over the indicated immobilised ACE2 variants. The right panels show an expanded view of the dissociation phase. The blue lines show fits used for determining the k_{on} and k_{off} .